Power exhaust by core radiation at COMPASS tokamak

M. Komm[1], **D. Mancini**[2], **M. Morbey**[3], **J. Cavalier**[1], **J. Adamek**[1], **M. Bernert**[4], **P. Bilkova**[1], **P. Bohm**[1], **D. Brida**[4], **O. Février**[5], **S. Henderson**[6], **M. Hron**[1], **M. Jerab**[1], **M, Imrisek**[1,7], **L. Kripner**[1,7], **D. Naydenkova**[1], **R. Panek**[1], **M. Sos**[1], **P. Vondracek and the EUROfusion MST1 team**[8]

[1] Institute of Plasma Physics of the CAS, Za Slovankou 3, 182 00 Prague 8, Czech Republic
[2] Consorzio RFX, Padua, Italy
[3] Science and Technology of Nuclear Fusion Group, Eindhoven University of Technology, Eindhoven, The Netherlands
[4] Max-Planck-Institut fur Plasmaphysik, 85748 Garching b. Munchen, Germany
[5] Ecole Polytechnique Federale de Lausanne (EPFL), Swiss Plasma Center (SPC), 1015 Lausanne, Switzerland
[6] Culham Sci Ctr, CCFE, Abingdon OX14 3DB, Oxon, England
[7] Faculty of Mathematics and Physics, Charles University, Prague, 12116, Czech Republic
[8] See author list of "B. Labit et.al. Nucl. Fusion 59 (2019) 086020

E-mail: komm@ipp.cas.cz

Abstract. Substantial power dissipation in the edge plasma is required for the safe operation of ITER and next-step fusion reactors, otherwise unmitigated heat fluxes at the divertor plasma-facing components (PFCs) would easily exceed their material limits. Traditionally, such heat flux mitigation is linked to the regime of detachment, which is characterised by a significant pressure gradient between upstream and downstream scrape-off layer (SOL). However, the physics phenomena responsible for power dissipation and pressure loss are distinctly different, especially when the power dissipation is achieved by impurity seeding. In principle, it is possible to achieve substantial mitigation of the heat fluxes while maintaining conservation of the pressure along the open field lines in the SOL. This regime can be accessed by injection of medium- or high-Z impurities, which mostly radiate inside the last closed flux surface. The critical question related to such an approach is the effect on confinement and perspective fusion power generation in future thermonuclear reactors.

In this work, we report on experiments at COMPASS tokamak, where neon and argon impurities were injected in ohmic or NBI-heated low confinement plasmas. With appropriate seeding waveform, stable scenarios were achieved, avoiding the radiative collapse of plasmas. Significant reduction of heat fluxes at the outer target was observed, with heat flux pattern similar to the one previously achieved by nitrogen seeding. The reduction of downstream pressure was, however, accompanied by an equal reduction of upstream pressure, indicating that the power dissipation occurred inside the separatrix. Indeed, the impurity cooling is causing a significant drop of edge temperature; however, the effect in the plasma centre is much less pronounced.

Submitted to: *Nuclear Fusion*

1. Introduction

Future thermonuclear reactors will require a strong power dissipation in the edge plasma in order to keep plasma heat fluxes at plasma-facing components within their material limits. ITER baseline scenario expects up to 70% of the power crossing the separatrix to be radiated in the scape-off layer (SOL) [1]. The conditions expected in the European DEMO concept are even more challenging — a substantial part of the power (65%) will have to be dissipated even before it reaches the separatrix, so that in total 95% of the power deposited to the plasma by either auxiliary heating or fusion reactions is dissipated [2]. Significant power dissipation can be achieved by the introduction of impurities in the plasma [3], which act as strong radiators. In present tokamaks, the majority of experiments is focused on radiation in the SOL, including real-time feedback systems for the control of divertor heat flux or temperature [4]. This is motivated by the requirement of ITER tokamak. Light impurities such as $_7$N have proved to be the most suitable, as they tend to radiate at temperatures relevant for SOL and divertor conditions [5].

However, as mentioned earlier, a DEMO reactor will require a significant dissipation of the power inside the separatrix, which can be achieved by application of medium- ($_{10}$Ne, $_{18}$Ar) or heavy-Z ($_{36}$Kr, $_{54}$Xe) impurities. Ideally, this dissipation should occur in a narrow mantle between the pedestal top and the separatrix, so that core confinement would not be affected. Experiments with medium- and high-Z impurities have been performed at JET with carbon wall, with promising results in terms of confinement and heat flux mitigation [6][7][8] as well as ELM size [9]. More recent experiments with metallic PFCs and neon seeding at JET [10] and AUG [11] reported observations of localised radiation around the X-point location with evident degradation of pedestal parameters. However, the core temperature sometimes increased and energy confinement time remained approximately constant (JET) or even slightly improved (AUG).

In this work, we present the results of similar experiments at COMPASS tokamak, where neon or argon was injected in low confinement plasmas. Due to the relatively low electron separatrix temperatures ($T_{e,sep} \sim 50\,eV$), it is expected that the majority of power will be dissipated from inside the separatrix. This work complements previous experiments with nitrogen seeding [12], where significant heat flux reduction was achieved and two novel models of divertor heat flux footprint characterisation were proposed.

This work is organised as follows: the overview of experiments with argon and neon seeding is described in Sec. 2, the effects of seeding on the core plasma are presented in Secs. 3 and 4. The effects on divertor heat fluxes are discussed in Sec. 5.

2. Low confinement scenario

The impurity was injected in a series of otherwise identical attached ohmically heated or NBI-assisted low confinement mode discharges ($I_p = -210\,kA, B_T = -1.38\,T, n_e = 5 \times 10^{19}\,m^{-3}$), which was based on the scenario used in [12]. The gas inlet for impurity injection was located in the divertor at $R = 500\,mm$, just outside the outer strike point. The
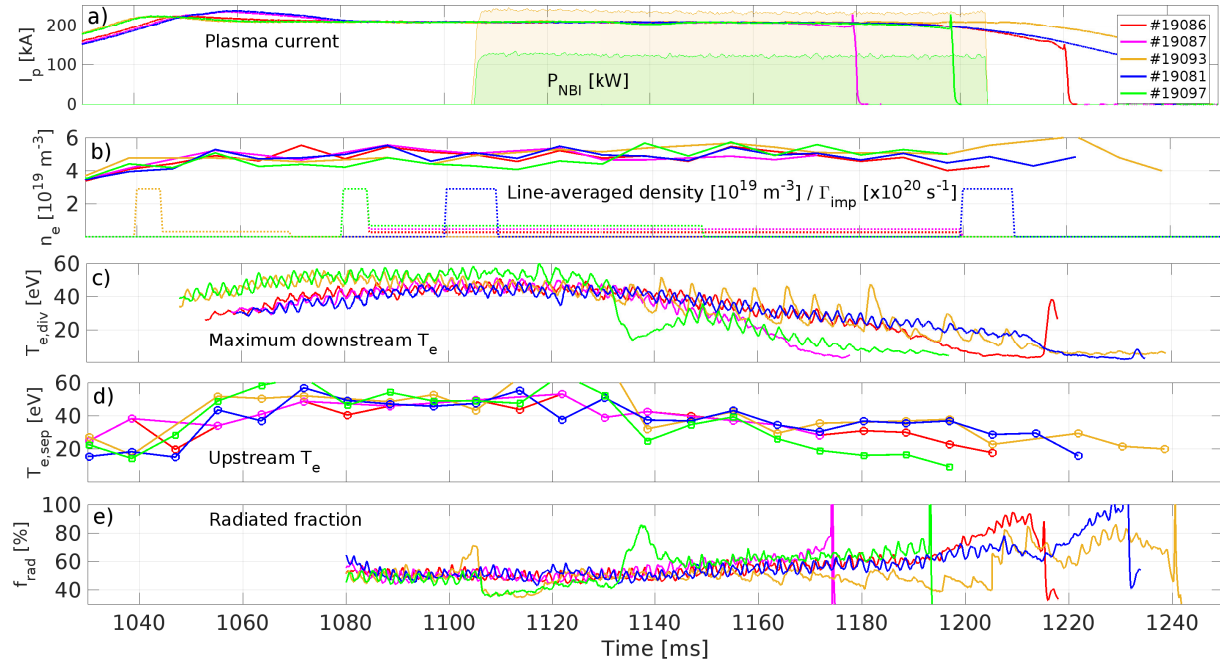
Figure 1. Overview of discharges with variable amount of impurity seeding showing evolution of plasma current I_p, line-averaged density n_e, maximum electron temperature measured by divertor probes at the outer target $T_{e,div}$, upstream separatrix electron temperature measured by HRTS $T_{e,sep}$ and radiated fraction f_{rad}.

injection was controlled by a pre-programmed piezoelectric valve. This valve requires an initial full opening for ~ 5 ms in order to ensure its proper functionality (so-called *pre-puff*). In the first attempts with neon seeding, it was observed that the amount of impurity introduced in the vessel during such a pre-puff was sufficient to cause a radiative collapse of the plasma. This issue was resolved by a reduction of the back-pressure in the gas reservoir, which is connected to the seeding valve — from 1.5 to 0.5 bar. After the pre-puff, a constant amount of impurity was injected into the plasma. By adjusting the rate and duration of the seeding, it was possible to avoid a disruption and achieve a scenario with full plasma flat-top and significant increase in radiated power (see Fig. 1). The upstream SOL collisionality prior to seeding was in the range of $\nu^*_{SOL} \sim 2\text{-}3$ ($\nu^*_{SOL} = 10^{-16} \, n_{sep} \, L_{con} \, / \, T^2_{e,sep}$ [13], where L_{con} is the connection length). The discharges used in the further analysis are listed in Table 1.

The selection of discharges allows the assessment of several aspects of impurity seeding. Discharges #19086 and #19087 are identical except for the argon seeding rate. The higher amount of seeding provoked a disruption at $t = 1180$ ms, indicating the upper limit of the seeding, which can be applied. Discharge #19081 had argon seeding applied in a series of discreet puffs, allowing thus to evaluate the time constant related to the effect of impurities in the plasma. The first puff at t=1100-1110 ms is causing gradual degradation of both upstream and downstream temperature with no signs of recovery before the end of discharge. Similar effect is seen in #19093, which had only short seeding waveform at the beginning of the discharge. This suggests that unlike nitrogen (as reported in [12]), noble gases are fully recycling and therefore the time constant of their removal is very long, longer than the

Table 1. List of discharges performed with neon and argon seeding seeding. Γ_{imp} is the seeding rate of impurity in atoms per second, t_{start} and t_{stop} denote the beginning and end of impurity seeding waveform. P_{NBI} is the maximum power deposited by the NBIs and t_{disr} the time of disruption.

Discharge	Impurity	Γ_{imp} [s^{-1}]	t_{start} [ms]	t_{stop} [ms]	P_{NBI} [kW]	t_{disr} [ms]
#19081	argon	2.9×10^{20}	1100	1110	0	1235
#19086	argon	0.27×10^{20}	1080	1200	0	1220
#19087	argon	0.47×10^{20}	1080	1200	0	1180
#19093	argon	0.30×10^{20}	1040	1070	230	1245
#19097	neon	0.67×10^{20}	1080	1150	120	1195

duration of the discharge. Similar results were observed, e.g. at Alcator C-mod [14]. This makes such impurities impractical for applications in real-time feedback systems for divertor heat flux control on machines with short pulses [15]. Discharge #19093 had a slightly higher seeding rate than #19086; however, an additional 230 kW of NBI power was deposited to the plasma, which allowed to extend the discharge duration and complete the ramp-down. Finally, #19097 represents an example of neon seeded discharge with only a moderate amount of deposited NBI power (120 kW). The seeding rate (in atoms per second) is higher than in #19087; however, the discharge survives practically until the end of flat-top. Note that neon as a lighter impurity has a lower cooling factor than argon for most temperatures [3].

3. Plasma cooling

With respect to medium Z impurities, the important question is where is the impurity radiation emitted. In principle, one can calculate the temperature dependence of cooling factors (as presented, e.g. in Fig. 1 in [3]) and simply map them to the temperature profiles in confined plasma and SOL. However, such a picture would be incomplete, since it neglects transport effects [5] and any change of plasma parameters due to radiation. A purely empirical approach consists of a comparison of the temperature profiles before and during seeding, as shown in Fig. 2. Time evolution of temperature at different ρ (ρ is the normalised poloidal flux coordinate) presented in Fig. 2 A and Fig. 2 C shows that a significant effect of the impurity seeding is visible for $t > 1160\,\text{ms}$ and $\rho \geq 0.5$, which corresponds to temperatures $T_{\text{e}} \leq 400\,\text{eV}$ for both argon and neon seeding.

The radial temperature profiles (Fig. 2 B and Fig. 2 D) suggest that in case of argon seeding, the temperature gradient in the core is not strongly affected, but the entire profile is shifted downwards. Neon seeding results in more complex change of the temperature profile. The reduction of temperature at the LCFS is in both cases significant - from $\sim 50\,\text{eV}$ to ~ 10 eV.

The effect of argon seeding on energy confinement time τ_{E} is presented in Fig. 3. τ_{E} is calculated using the formula

$$\tau_{\text{E}} = \frac{W_{\text{plasma}}}{P_\Omega + P_{\text{NBI}} - \mathrm{d}W_{\text{plasma}}/\mathrm{d}t}, \tag{1}$$
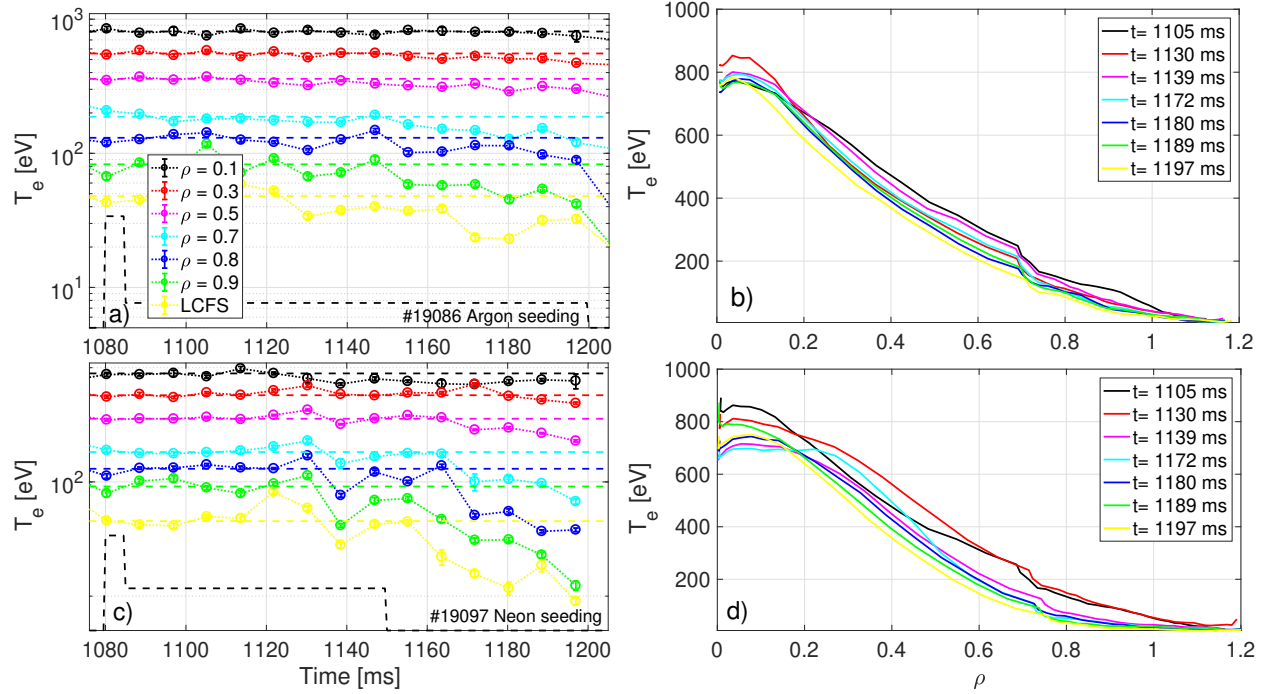
Figure 2. Temperature changes due to argon (A-B) and neon (C-D) seeding. Dashed black line indicates the seeding waveform.
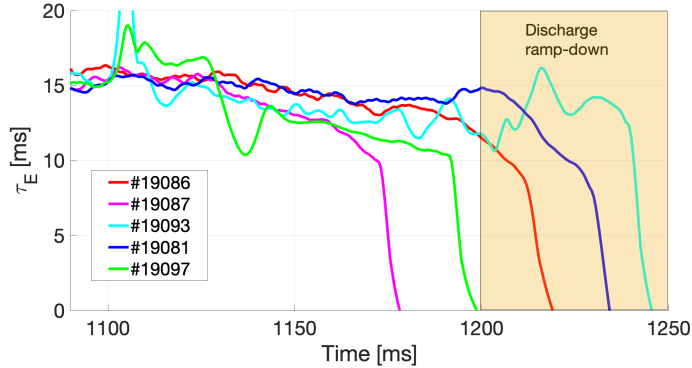
Figure 3. Energy confinement time τ_E evolution during discharges with argon seeding.

where W_{plasma} is the plasma energy calculated by EFIT, P_Ω the Ohmic power and P_{NBI} the auxiliary heating by NBI. In the calculation of P_{NBI}, the CX losses and shine-through was included — estimated to remove 40% of the power injected into the plasma [16]. The calculation does not take into account the effect of the finite fast ion slow downtime, which results in an artificial peak of τ_E at the beginning and end of the NBI heated phase in #19093. All the discharges start with a τ_E of 15 ms, which is being gradually degraded by $\sim 30\%$ to 10 ms. Beyond this value, a quick degradation of confinement occurs either due to a radiative collapse of the plasma or during plasma ramp-down ($t > 1200\,\text{ms}$).

Similarly, the high confinement factor H98(y,2) [17] tended to be rather resistant to the impurity seeding, as shown in Fig. 4. For completeness, a trace of a nitrogen seeded discharge
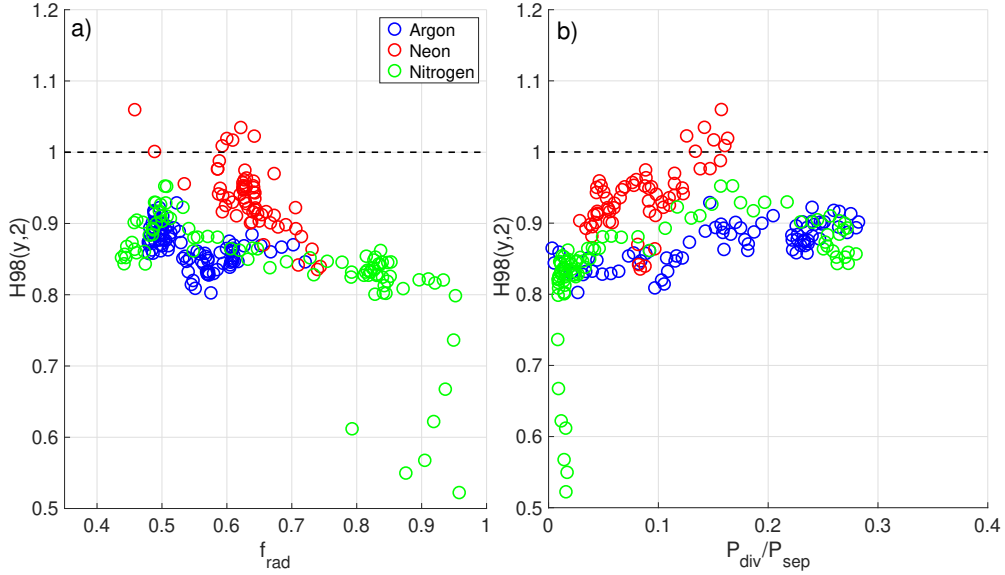
Figure 4. H98(y,2) factor dependence on f_{rad} (A) and the fraction of power reaching the outer target (B).

from [12] is plotted too. This case exhibits significant degradation of H98 when $f_{\text{rad}} > 0.9$ is reached. Note that the pre-seeding value of H98 in all discharges is somehow higher than expected for low confinement mode plasmas, however this behavior is consistent with values reported already at COMPASS-D [18]. The highest values of H98 were observed in the neon seeded discharge, however, they were unlikely to be caused by the action of impurity (in contrast with observations on other machines [19]), since the elevated values are observed before the effect of neon seeding is manifested in the divertor (as can also be seen in Fig. 3). Most probably, the alteration in pre-seeding values of H98 in studied discharges is caused by varying wall condition.

The pressure loss between the upstream and downstream location in the SOL is considered as the definition of detachment [20]. An example of the evolution of both quantities is shown in Fig. 5. The pressure was calculated in the same manner as in [12]: the upstream pressure was obtained from HRTS profiles interpolated to the location of separatrix (as calculated by EFIT). The downstream pressure is the maximum pressure measured at the outer target by an array of Langmuir and ball-pen probes [21]. The effect of argon and neon seeding is visible both on upstream and downstream pressures, with a reduction of factor $\sim 3\times$. Their ratio remains approximately constant in time, which suggests that the pressure loss in the SOL is, in fact, negligible — the power dissipation occurs inside the separatrix.

Neon seeding results in a sudden drop of pressures at t ~ 1135 ms, which is followed by a partial recovery. This is most probably an effect of the seeding pre-puff and suggests complex effect of neon on the plasma as it propagates from the divertor region into the confined plasma.

Note that only relative changes of $p_{\text{down}}/p_{\text{up}}$ are relevant since the determination of separatrix location can exhibit a systematic offset [22], which influences the absolute value of p_{up}. This is a known caveat of equilibrium reconstruction codes, which is commonly assessed
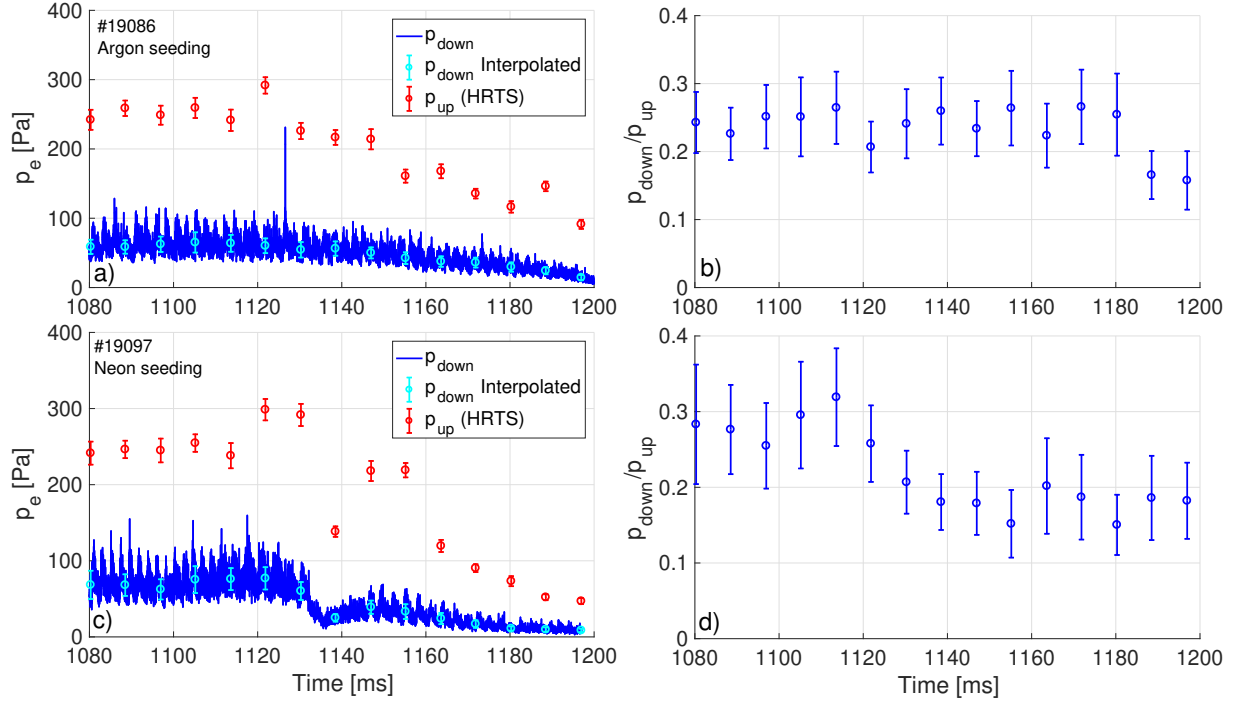
Figure 5. Upstream and downstream electron pressure evolution during argon (A-B) and neon (C-D) seeding.

by an estimation of the separatrix temperature using the 2 point model for the conduction-limited regime. However, since COMPASS mostly operates in the sheath-limited regime or in the transition between these two regimes, such an approach is not applicable.

4. Impurity radiation

The radiation of impurities was monitored by an array of AXUV photodiodes [23], which allowed to obtain poloidal maps of radiated power by tomographic reconstruction. Time snapshots of reconstructed radiation during argon and neon seedings are shown in Fig. 6. It can be seen that the reconstructed radiation profiles during argon seeding (Figs. 6 A–D) is localised in a relatively narrow mantle located around $\rho \sim 0.5$ (as indicated by white dashed lines), which is consistent with the location of cooling as observed by HRTS. In the case of neon (Figs. 6 E–H), the radiation pattern is significantly broader and gradually expands also into the plasma centre. This difference is most likely caused by different transport of the two species and the temperature dependence of their cooling factors L_z (see Fig. 1 in [3]).

The measurements of AXUV photodiodes are also used to calculate the total radiated power P_{rad} and radiated fraction f_{rad} (used later in this text). During the analysis of discharges with argon and neon seeding, it was observed that f_{rad} is systematically higher than in previous discharges with nitrogen seeding, which were presented in [12]. This was also true for initial phases of discharges prior to impurity seeding. Subsequent analysis of *standard discharges* (Ohmic discharges, which are ran at the beginning of each experimental day without any
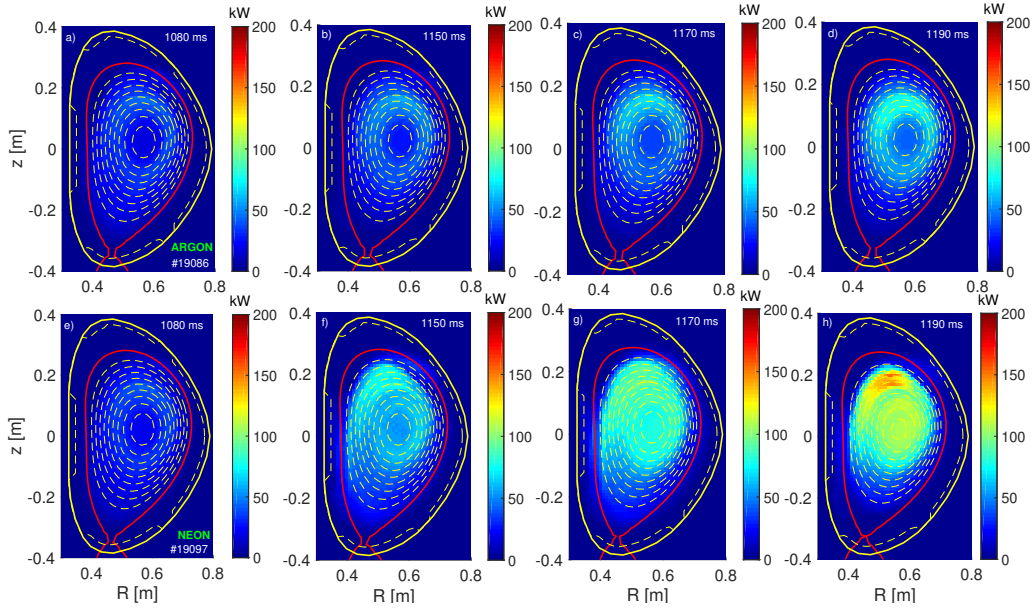
Figure 6. Radiation of argon (#19086, top row) and neon (#19097, bottom row) during impurity seeding experiments, as measured by AXUV photodiodes. White dashed lines indicates magnetic flux surfaces by step of $\Delta\rho = 0.1$, red line indicates the separatrix.

impurity seeding) revealed that the source of the effect was a gradual degradation of sensitivity of the AXUV sensors, as shown in Fig. 7. This degradation can be caused by various effects (see their discussion in [24]), however in COMPASS it is assumed that the primary cause was exposure of AXUV diodes during boronisations, as their protective shutters were not functional over some period of time. Coincidently, the sensors were replaced soon after the nitrogen seeding campaign and their shutters were repaired and no changes in the sensitivity were observed since then. Note that there is a significant spread in the measured radiation, which is to some extend correlated with the number of plasma seconds achieved since boronisation. The campaign with neon and argon seeding was performed shortly after the end of summer shutdown without any preceding boronisation, which is probably responsible for overall high detected radiation.

The scatter in the measurements during standard discharges did not allow for precise determination of AXUV photodiodes sensitivity during nitrogen seeding experiments. Instead, the sensitivity was estimated in discharge #15977, where intensive nitrogen seeding resulted in a disruption. P_{rad} was rescaled so that $f_{rad} \sim 1$ just before the disruption. This introduced a scaling factor of 5.4 for P_{rad} in the nitrogen seeded discharges.

5. Divertor heat flux footprint

The divertor conditions were diagnosed by a combined array of Langmuir and ball-pen probes. Fig. 8 shows the evolution of the ion saturation current density j_{sat}, electron temperature T_e and parallel heat flux $q_{||}$ during argon seeding. The electron temperature was obtained using $\alpha = 1.4$ and $q_{||}$ was calculated using $\gamma = 11$ [25].
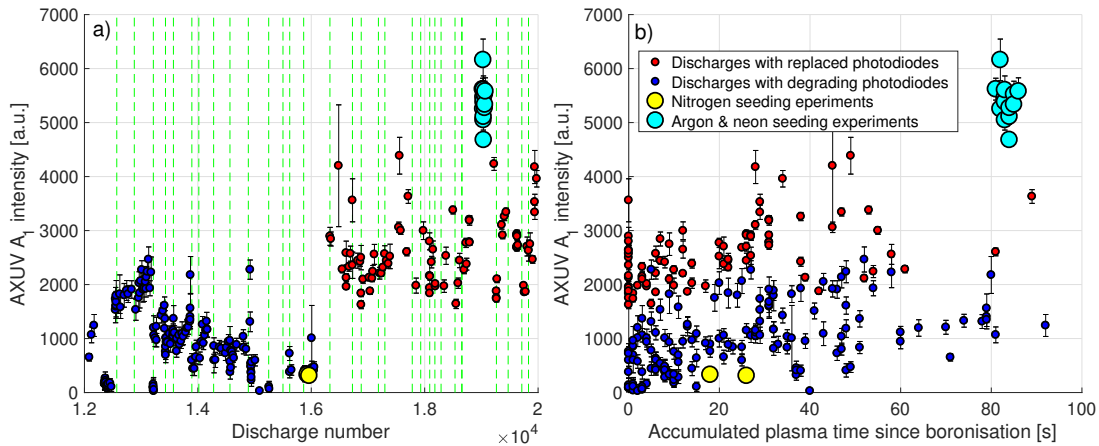
Figure 7. Measured intensity of radiation on the A_1 AXUV chord in standard discharges in COMPASS showing degradation of the sensitivity for discharges before and after replacement of the photodiodes Boronisations are marked by vertical green dashed lines. Standard shots performed during experiments with nitrogen, neon and argon seeding are highlighted.
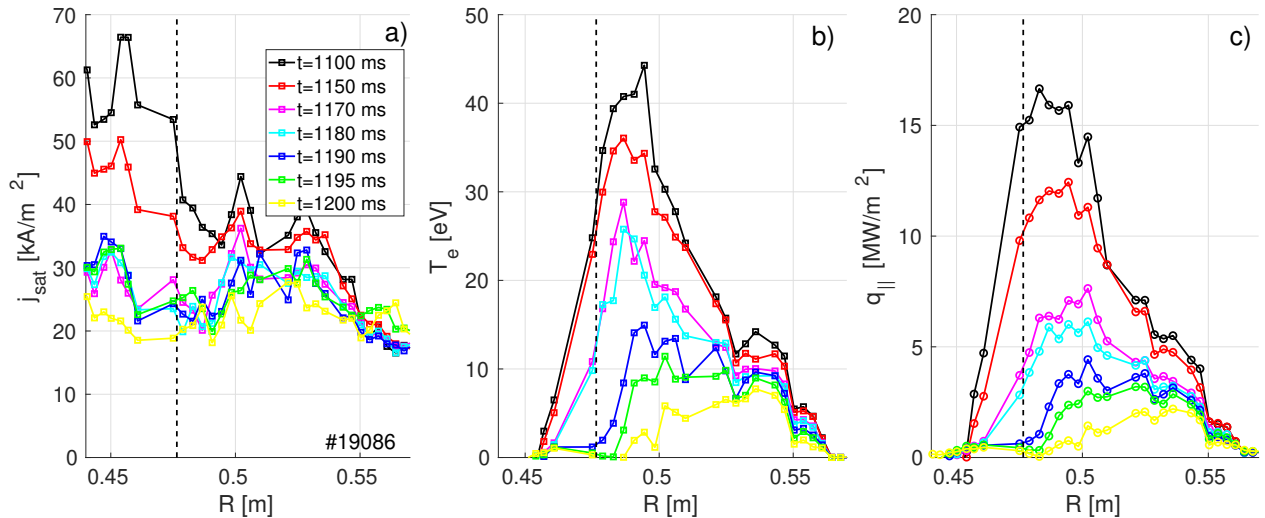
Figure 8. Divertor conditions during argon seeding in discharge #19086. Vertical dashed lines indicate location of the OSP as calculated by magnetic equilibrium reconstruction.

The effect of seeding is visible mainly on the temperature profile, with peak temperatures dropping from 45 eV to less than 10 eV. Also, the location of maximum T_e is shifting further away from the strike point, which is a common feature observed in other tokamaks during detachment experiments [26] and modelling [1]. Given the results presented in the previous section, the shift is still somehow surprising in our particular case of heat flux reduction, which is not accompanied by detachment. If we consider that all the power dissipation occurs inside the separatrix, one may expect the temperature (and heat flux) profile to be simply scaled down by a constant factor. However, there are two effects, which may be responsible for this unexpected result. The first is the role of the E×B drift, which is significant in attached
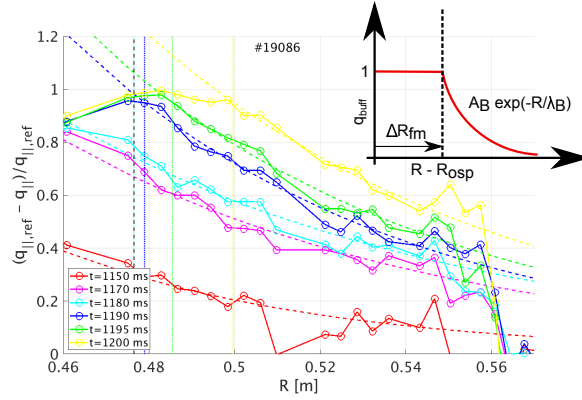
Figure 9. Buffered heat flux q_{buff} profiles at different times in discharge #19086. Vertical dashed lines mark the full mitigation width ΔR_{fm} for each profile.

discharges in COMPASS due to its relatively large T_e and small B field [27]. The reduction of the T_e during seeding should also reduce the E field, resulting in a smaller drift velocity. Thus, the footprint, which has been initially affected by the presence of the drift may appear to be deformed, when the drift vanishes. However, dedicated simulations of the edge plasma (e.g. using SOLPS code) would be needed to verify this hypothesis.

The second effect causing deformation of the footprint may be collisional processes occurring close to the strike point, where the connection length is the longest (9 m). These processes typically become visible for $T_e < 10$ eV [28].

The deformation of the footprint is further illustrated in Fig. 9, where the buffered heat flux q_{buff} is presented. The definition of q_{buff} is the same as in [12]:

$$q_{\text{buff}}(R, t) = (q_{\text{ref}}(R) - q_{||}(R, t))/q_{\text{ref}}(R), \tag{2}$$

where $q_{\text{ref}}(R)$ is the reference radial profile of parallel heat flux obtained prior to seeding. q_{buff} is clearly not constant with R but can be approximated by an exponential dependence $q_{\text{buff}} = A_B \exp(-(R - R_{\text{OSP}})/\lambda_B)$, where A_B is the *strike point heat flux reduction factor* and λ_B characterises the spatial extend of the buffering (dubbed *buffering decay length*).

In contrast to results with nitrogen seeding, for $t > 1180$ ms there is clearly a region just outside the strike point, where q_{buff} flattens at values close to 1. In this region, the heat flux is practically fully mitigated and clearly is not suitable for the exponential fitting of the profile. Therefore, a third parameter ΔR_{fm} is introduced — the distance from the strike point, where $q_{\text{buff}} > 0.95$ (dubbed *full mitigation width*) , which corresponds to 95% mitigation of the heat flux. The exponential fit was performed only for $R > R_{\text{OSP}} + \Delta R_{\text{fm}}$.

The evolution of the three parameters (A_B, λ_B and ΔR_{fm}) is shown in Fig. 10 as a function of the radiated fraction $f_{\text{rad}} = P_{\text{rad}}/(P_\Omega + P_{\text{NBI}})$ for selected discharges with argon (#19087), neon (#19097) and nitrogen (#15977) seeding. The evolution of the parameters has qualitatively a similar behaviour for all three injected impurities. High values of $A_B \sim 1$ are achieved at slightly lower f_{rad} for nitrogen seeding, in comparison to neon and argon. The dependence of the decay length of λ_B tends to follow a common trajectory. Note that the fitting provided reliable results only for profiles with maximum heat flux being at least 10%
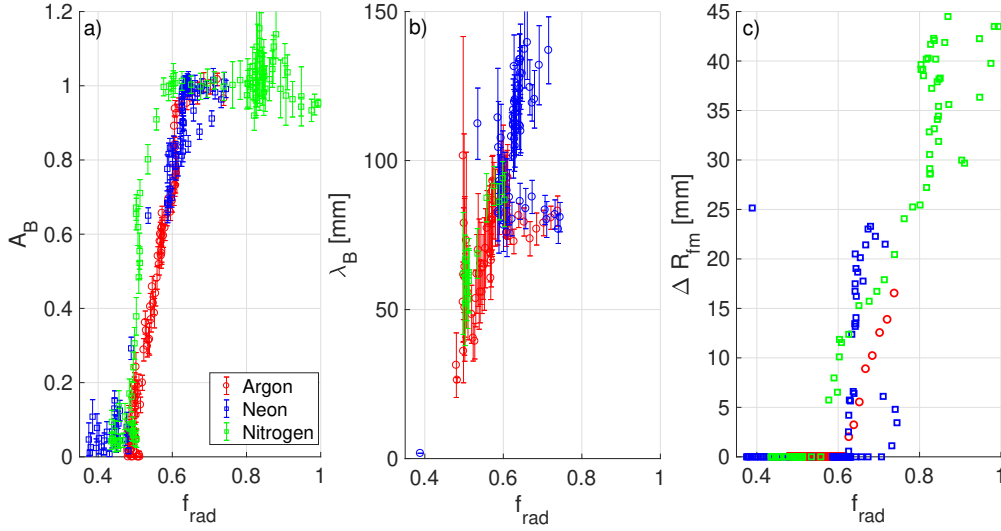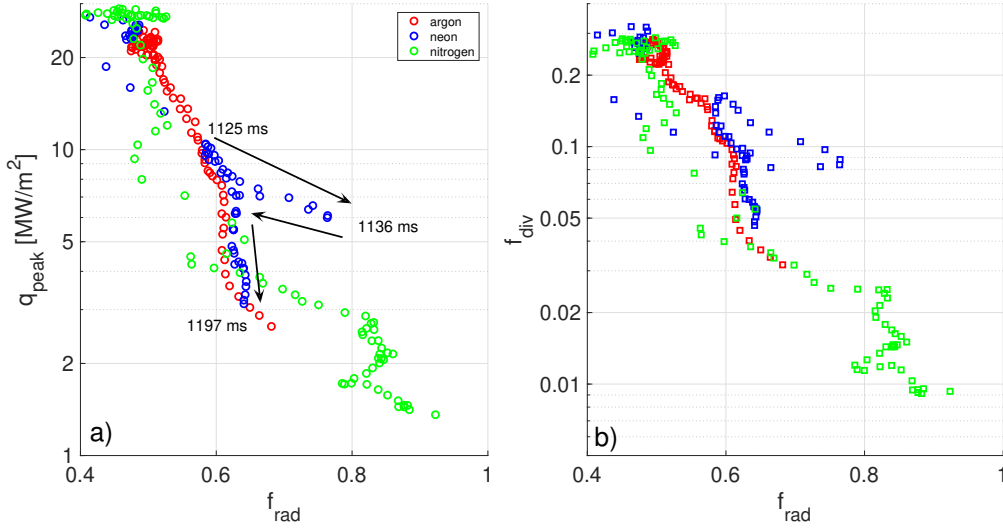
Figure 10. Dependence of divertor heat flux parameters A_B (strike point heat flux reduction factor), λ_B (buffering decay length) and ΔR_{fm} (full mitigation width) on the radiated fraction for discharges with argon (#19087), neon (#19097) and nitrogen (#15977) seeding.

of the reference peak heat flux. Also, the third parameter ΔR_{fm} shows similar trajectories for all three impurities, although with some scatter. Surprisingly, this parameter is present also for nitrogen seeding, however only in discharges with high seeding rate (such as #15977) and could not be immediately identified in discharges with lower seeding rates, such as the one analysed in Fig. 17 in [12].

Similarly to the analysis presented in [12], the generic parameters characterising the divertor heat flux footprint (q_{peak}, f_{div} and S_f) were calculated and their dependence on radiated fraction f_{rad} is shown in Fig. 11. The discharges with different injected species seem to follow a qualitatively similar trajectory, which is characterised by a steady reduction of q_{peak} with increasing f_{rad}, followed by abrupt mitigation of the heat flux. However, the location of this abrupt change of slope appears to be specific for each impurity, occurring at smaller f_{rad} for nitrogen seeded discharges than for heavier impurities. The dependence of f_{div} on f_{rad} seems to converge onto a common trajectory for $f_{div} < 0.05$. There is an interesting behaviour of the neon seeded discharge (#19097). It appears that this discharge was probably close to a disruption around $t = 1136\,\mathrm{ms}$, where the radiated fraction has reached almost 80%. This was most probably the effect of pre-puff (since there was no sign of the neon injection on divertor parameters prior to this time), however, then the radiation decreased again and continued on the trajectory similar to the argon seeded discharge (#19087) until it disrupted at the lower value of $f_{rad} \sim 65\%$.

There is a difference regarding the limits of heat flux mitigation which can be achieved by individual impurities. All three discharges presented in Fig. 11 terminated by a disruption, most probably due to radiative collapse of the plasma. However, it is visible, that nitrogen was able to achieve stronger mitigation of q_{peak} (down to 1.5 MW/m^2) then neon and argon (~ 3 MW/m^2).

Figure 11. Dependence of generic divertor heat flux parameters q_{peak}, f_{div} on the radiated fraction for discharges with argon (#19087), neon (#19097) and nitrogen (#15977) seeding

One important question with respect to the characterisation of the heat flux footprint is whether the maximum surface heat flux $q_{peak,surf}$ is proportional to the integral power reaching the divertor target P_{div}. In other words, despite the fact that the footprint becomes significantly deformed and the location of the maximum heat flux shifts further away from the strike point, is it still possible to consider a simple linear relation between these two quantities? With the available experimental data, it is possible to cross-check a simplified model, which is commonly used to predict the surface peak heat flux at the divertor:

$$q_{peak,surf} = \frac{P_{div} \sin \beta}{2\pi \lambda_q f_x R_t}, \tag{3}$$

where f_x is the flux expansion at the location of the maximum heat flux (which can be approximated as the location of outer strike point), β is the poloidal projection of angle of incidence between magnetic field line and the target. Together, these two parameters form the effective poloidal flux expansion $f_{pol,eff} = f_x / \sin \beta$. Note that the model assumes that $f_{pol,eff}$ is approximately constant in the proximity of the strike point. The power decay length λ_q can be obtained by fitting the (reference) heat flux profile by the so-called "Eich function" [29] (as it was performed in [12]) and correspond to λ_{int}, however in case of this scenario $\lambda_{int} \sim \lambda_q$ since the spreading factor S is negligible [12]. Finally R_t is the target radial coordinate. Using actual values $f_{pol,eff} = 25$, $\lambda_q = 4.0$ mm and $R_t = 0.477$ m, it is possible to compare the predictions of this model with experimental observations.

Figure 12 B shows the comparison of this model with experimental measurements of the surface heat flux (note that the probes allow calculating parallel heat flux $q_{||}$, which are then translated to surface heat flux using an angle of incidence of the magnetic field lines calculated by EFIT). While the linear relation between $q_{peak,surf}$ and f_{div} is well pronounced, the model under-estimates the absolute value by more than a factor 2 (cyan dashed line). However, the
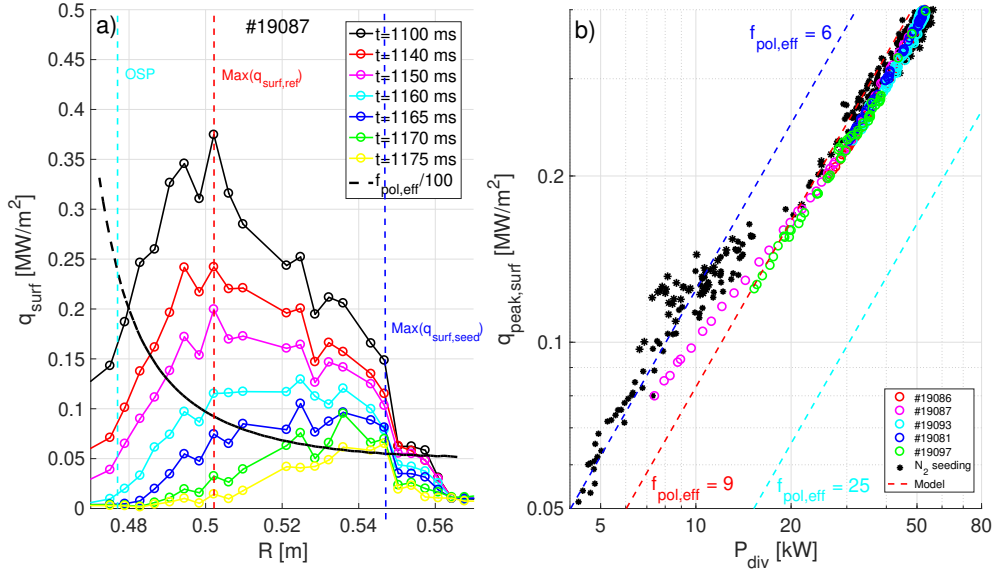
Figure 12. Spatial profiles of the surface heat flux q_{surf} (A), dependence of the peak heat flux q_{peak} on the fraction of power reaching the divertor P_{div}, including discharges with nitrogen seeding, which were reported in [12],

agreement significantly improves if instead of using the value of $f_{pol,eff}$ which corresponds to the location of the outer strike point, we employ value which corresponds to the actual location of the maximum of the surface heat flux (red dashed line). Figure 12 A shows that the radial of $f_{pol,eff}$ changes rapidly between these two locations, from the value of 25 (at OSP) down to 9 (at the maximum of the reference heat flux profile). This is caused by the proximity of the X-point to the divertor targets (the vertical distance was approximately 15 mm). During the course of the seeding, the maximum of the surface heat flux shifted further away from the OSP, into a location of further reduced $f_{pol,eff} = 6$ (blue dashed line). When this value was used in Eq. 3, the predicted values of $q_{peak.,surf}$ represent an upper limit of the experimental values of q_{surf}. This adjustment had to be made because the assumption of the simplified model, constant $f_{pol,eff}$ in the proximity of the strike point, is not satisfied in COMPASS due to the close proximity of X-point to the divertor target.

6. Conclusions

Experiments with argon and neon injection into low confinement plasmas in the COMPASS tokamak have demonstrated that the phenomena of divertor heat flux mitigation and plasma detachment are not necessarily as closely linked as it is commonly assumed. Despite a reduction of the target heat fluxes by a factor 10, there was no significant change of p_{down}/p_{up} during the discharge. This is because most of the radiation occurred inside the separatrix, which was confirmed by HRTS and AXUV photodiodes measurements. In light of these observations, it is natural to ask which parameters are of key importance in the challenge of power exhaust. From the perspective of ITER operation (with stringent material limits for divertor monoblocks on one side and the requirement for reaching $Q = 10$ on the other), it is

the peak heat flux at the target, which, as was shown, scales linearly with the power reaching the divertor, and the confinement represented by H98(y,2) factor [17]. As shown in Fig. 4, the variation of H98 in studied discharges appears to be modest in most cases.

With respect to the reduction of peak heat flux at the outer divertor, nitrogen proved to achieve best results (as shown in Fig. 11 A), which was expected given the size of the machine and plasma temperatures. However, the results from neon and argon seeding does seem not to exhibit significant difference in comparison with nitrogen seeding, which is perhaps the most surprising result of the study, since the radiative cooling occurs in different locations of the plasma.

The analysis of the deformation of the heat flux footprint has confirmed that the buffered heat flux can be approximated by a slow exponential decay along the outer target. However, contrary to results with nitrogen seeding, a new parameter had to be added to obtain a reliable approximation of q_{buff}. This parameter ΔR_{fm} (full mitigation width) describes the area in the vicinity of the strike point, where the heat flux is practically fully mitigated.

The experimental data provided verification of a simplified model of peak heat flux prediction, which is commonly used for design purposes, e.g. for the COMPASS-U tokamak [30]. This study confirmed that despite significant deformation of the footprint and shift of the location peak heat flux, it is still reasonable to assume a linear relationship between the power reaching the divertor and the surface peak heat flux. The deviations from the model can be explained by a variation of the effective flux expansion along with the target. This variation is more pronounced on COMPASS than on most contemporary machines and ITER predictions; however, it is relevant to some of the alternative divertor configurations, which employ secondary X-points in the vicinity of the targets. Our results show that if the spatial scale of $f_{pol,eff}$ variation is comparable or smaller than the downstream power decay length, it is important to take this effect into account.

The injection of neon and argon has always led to a progressive decrease in energy confinement time. When this reduction exceeded 30%, the plasma was prone to radiative collapse. In case of argon, the central temperature and density were only weakly affected by the presence of the impurities, neon seeding resulted in their more pronounced reduction.

The results reported in this work represent first successful power exhaust experiments with neon and argon seeding in COMPASS. Naturally, the relevance towards next-step devices is limited by the fact that the seeding was performed only in low confinement plasmas. So far any attempts to seed impurities into H-mode plasmas resulted in transition to unstable ELM-free discharge and a subsequent disruption or HL transition, which is probably caused by a lack of auxiliary heating. However, we plan to revisit impurity seeding in H-mode once the new 1 MW NBI will be commissioned.

Acknowledgments

[1] R.A. Pitts et al., Nucl. Mat. Energy 20 (2019) 100696.

[2] R.P. Wenninger et al., Nucl. Fusion 54 (2014) 114003.

[3] T. Putterich et al., Nucl. Fusion 59 (2019) 056013

[4] A. Kallenbach et al. Nucl. Fusion 55 (2015) 053026

[5] A. Kallenbach et al. Plasma Phys. Control. Fusion 55 (2013) 124041

[6] P. Dumortier et al. Plasma Phys. Control. Fusion 44 (2002) 1845-1861

[7] G. P. Maddison et al. Nucl. Fusion 43 (2003) 49-62

[8] J. Rapp et al. Nucl. Fusion 44 (2004) 312

[9] G. P. Maddison et al. Plasma Phys. Control. Fusion 45 (2003) 1657-1669

[10] S. Gloeggler et al., Nucl. Fusion 59 (2019) 126031

[11] M. Bernert et al. Nucl. Mat. Energy 12 (2017) 111-118

[12] M. Komm et al., Nucl. Fusion 59 (2019) 106035

[13] P.C.Stangeby, *The Plasma Boundary of Magnetic Fusion Devices*, Bristol, Institute of Physics (2000)

[14] M. Reinke, J. Nucl. Mat. 415 (2011) S340-S344

[15] I. Khodunov et al., submitted to Plasma Phys. Control. Fusion (2020)

[16] J. Urban et al., Czech. J. Phys. 56 (2006) B176-B181

[17] ITER Physics Expert Group on Confinement and Transport, Nucl. Fusion 39 (1999) 2175

[18] P.G. Carolan et al. Plasma Phys. Control. Fusion **36** (1994) A111-A116

[19] J. Ongena et al. Phys. Plasmas 8 (2001) 2188

[20] A.W. Leonard et al. Plasma Phys. Control. Fusion **60** (2018) 04401

[21] J. Adamek et al., Nucl. Fusion 57 (2017) 116017

[22] K. Jirakova et al. J. Instr. 14 (2019) C11020

[23] M. Imrisek et al., Nukleonika 61 (2016) 404-408

[24] M. Bernert et al., Rev. Sci. Instr. 85 (2014) 033503

[25] P. Vondracek, *Plasma heat flux to solid structures in tokamaks*, dissertation thesis https://is.cuni.cz/webapps/zzp/detail/123000/.

[26] A. Loarte et al. Phys. Plasmas 18 (2011) 056105

[27] C.G. Silva et al., *J. Nucl. Mater.* **266-269** (1999) 679-684

[28] P.C. Stangeby, Plasma Phys. Control. Fusion 60 (2018) 044022

[29] T. Eich et al., Nucl. Fusion **53** (2013) 093031

[30] R. Panek et al., Fus. Eng. Design, 123 (2017) 03